Journal of Power Sources 419 (2019) 58–64

Contents lists available at ScienceDirect

Journal of Power Sources

journal homepage: www.elsevier.com/locate/jpowsour

A novel non-porous separator based on single-ion conducting triblock copolymer for stable lithium electrodeposition

Kun-Lin Liu[a], Chung-Hsiang Chao[d], Hsin-Chieh Lee[a], Cheng-Si Tsao[a,e], Jason Fang[d], Nae-Lih Wu[b,c], Chi-Yang Chao[a,c,*]

[a] Department of Materials Science and Engineering, National Taiwan University, Taiwan
[b] Department of Chemical Engineering, National Taiwan University, Taiwan
[c] Advanced Research Center for Green Materials Science and Technology, National Taiwan University, Taiwan
[d] Industrial Technology Research Institute, Taiwan
[e] Institute of Nuclear Energy Research, Atomic Energy Council, Taiwan

HIGHLIGHTS

- Single ion conducting triblock copolymer is synthesized via anionic polymerization.
- SII membrane exhibits an interpenetrated bicontinuous network microstructure.
- SII-LE membrane shows high conductivity and high T_{Li}^{+} at room temperature.
- More than 500 h lithium cycle life time is achieved upon galvanostatic cycling.
- SII-LE membrane stabilized lithium electrodeposition.

GRAPHICAL ABSTRACT

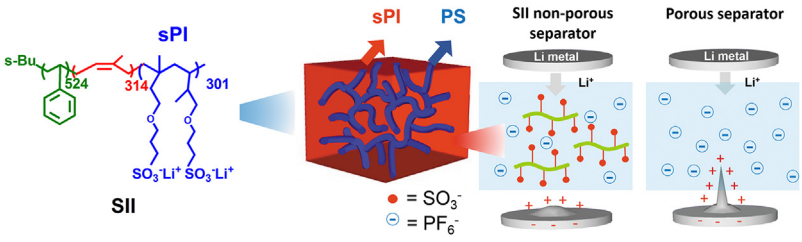

ARTICLE INFO

Keywords:
Lithium metal batteries
Dendrites
Polyelectrolyte
Block copolymer
Separator

ABSTRACT

A novel non-porous separator that possesses an outstanding lithium transference number (0.92) and effectively suppresses lithium dendrite formation upon lithium deposition is developed. The separator is made of triblock copolymer poly(styrene-*block*-isoprene-*block*-sulfonated isoprene) bearing pendant lithium sulfonates and, while taking up only 30 wt% liquid electrolyte (1 M Lithium hexafluorophosphate in ethylene carbonate/diethyl carbonate/ethyl methyl carbonate (v/v/v = 4/3/3)), it allows a high ion conductivity of 10^{-4} S cm^{-1}. With good mechanical strength and processing feasibility, the new non-porous separator is shown to enable dendrite-free lithium electro-deposition and stripping with flat overpotential profiles upon prolonged galvanostatic cycling of the lithium symmetrical cells in the carbonate-based electrolyte.

1. Introduction

Lithium metal batteries (LMBs) employing lithium metal as the anode is a promising approach to achieve high energy density for next generation energy storage devices since volume and weight of a battery could significantly decrease in comparison with the commercial lithium ion batteries (LIBs) using graphite as the anode [1–3]. The commonly adopted cell assembly for LMBs is similar to commercial LIBs, in which liquid electrolytes are absorbed within a mesoporous separator locating between anode and cathode. Nevertheless, lithium dendrite growth is

* Corresponding author. Department of Materials Science and Engineering, National Taiwan University, Taiwan.
E-mail address: cychao138@ntu.edu.tw (C.-Y. Chao).

https://doi.org/10.1016/j.jpowsour.2019.02.048
Received 9 October 2018; Received in revised form 1 February 2019; Accepted 15 February 2019
Available online 23 February 2019
0378-7753/ © 2019 Elsevier B.V. All rights reserved.

much more vigorous at the interface between lithium metal and liquid electrolyte upon battery cycling. Lithium dendrites may penetrate through the pores of the separator to cause internal short circuit, leading to severe safety issues [4,5]. Despite that significant progresses have been reported from a proliferation of studies on suppressing lithium dendrite in LMBs using the conventional mesoporous separators, including electrolyte additives, artificial solid electrolyte interphases (SEI) and geometry engineering on lithium metal [6–21], the intrinsic issues raised from the existence of pores remained un-resolved. The high porosity also requires the separator to adsorb a large amount of liquid electrolyte to achieve acceptable ion conductivity, thus resulting in another safety issue related to high flammability. On the other hand, pore-free gel type electrolytes as replacement of separator/liquid electrolyte system, suffer from poor mechanical strength and which are unable to block dendrite growth despite the absence of pores [22,23]. Additionally, gel electrolytes also need the presence of a large amount of solvent to attain good ion transport properties. Therefore, the use of non-porous separators was thought to be an appraisable approach in the aspect of suppressing lithium dendrite formation by retaining the mechanical superiority while avoiding the issues arising from the pores [24,25]. Recently, Li et al. suggested that a non-porous separator would have a better chance to limit dendrite growth comparing with a mesoporous one since heterogeneous diffusion of lithium ions associated with the pores could be avoided [24]. Nevertheless, the non-porous separators may entail challenges originating from the lack of pores, especially a decrement in ionic conductivity due to the absence of continuous conducting pathways; therefore, only very limited works have been conducted.

In this work, we develop a non-porous separator for the application in a LMB to simultaneously fulfil the following perquisites, including: (1) acceptable ionic conductivity upon low liquid electrolyte uptake, (2) good mechanical strength and easy processability to sustain the cell assembly process; and (3) capability to suppress lithium dendrite growth. Dendrite growth is suggested to be influenced complicatedly by a variety of factors based on several theoretical models, including mechanical properties, ionic conductivity and lithium transference number (T_{Li}^+) of the electrolyte, as well as the interface between electrolyte and lithium metal [26–29]. Among them, increasing T_{Li}^+ could effectively suppress dendrite growth as proposed by Chazalviel et al. [26] and Archer et al. [28,30,31]. Practically, polyelectrolytes bearing pendant lithium salts whose anions are anchored onto the polymer backbone would provide high T_{Li}^+, and thus are favourable to suppressing dendrite growth [25]. A thin layer of polyelectrolyte, e.g. Nafion, serving as a protective layer on top of lithium metal was demonstrated to remarkably improve the stability of the LMB by facilitating homogeneous deposition and stripping of lithium to suppress lithium dendrite [32]. The polyelectrolyte layer apparently needs to be sufficiently robust to prolonged cycling. Nafion, for instance, has been reported to swell in the ether-based electrolyte that is commonly used in the Li-S batteries, gradually losing the dendrite suppressing function upon cycling [33].

In order to concurrently realize the advantages of non-porous separators and the superiority of polyelectrolytes in the aspect of suppressing lithium dendrite, we hereby successfully develop a novel triblock copolymer poly (styrene-*block*-isoprene-*block*-sulfonated isoprene) termed as SII, whose chemical structure is depicted in Fig. 1 and fabricate the corresponding non-porous separator. SII is comprised of a terminal polystyrene (PS) segment with high T_g to provide mechanical strength of the separator, a central ductile polyisoprene (PI (1,4)) segment with low T_g to introduce flexibility and processability, as well as another terminal sulfonate polyisoprene (sPI) segment bearing pendant lithium sulfonates (SO_3Li) to offer immobile anions and dissociable lithium ions, which might also contribute to lithium ion conduction. This separator was found to exhibit microphase-separated microstructure possessing a continuous network of sPI domains enabling fast lithium ion transport. As a result, a high ionic conductivity can be achieved with only a limited amount (~30 wt%) of liquid electrolyte (LE, 1 M $LiPF_6$ in EC/DEC/EMC (v/v/v = 4/3/3)) uptake in this. The low liquid electrolyte uptake enables additional advantages including reduced flammability, improved mechanical strength and enhanced electrochemical stability. sPI is a single ion conducting polyelectrolyte enabling T_{Li}^+ close to 1 and effective dendrite suppression. Galvanostatic cycling of lithium symmetrical cells comprising of the SII separator demonstrate dendrite-free electrodeposition and stripping of lithium on the lithium metal surface along with outstanding electrochemical performance.

2. Experimental

2.1. Materials

Sec-butyl lithium (1.3 M in cyclohexane), styrene (99%), isoprene (99%), 9-Borabicyclo[3.3.1]-nonane solution (0.5 M in THF), H_2O_2 (30 wt% in H_2O), lithium *tert*-butoxide (99%), *di*-butyl magnesium (1.0 M in heptane) and methanol (anhydrous, 99.8%) are all purchased from Sigma-Aldrich. 1,3-propane sultone (99%) is purchased from Alfa Aesar. THF and toluene are dried over sodium before use. Styrene and isoprene are purified from *di*-butyl magnesium before use.

2.2. Synthesis and characterization of SII triblock copolymer

SII triblock copolymer is synthesized by anionic polymerization and the succeeding analogous chemistry following the routes illustrated in Fig. 1 All the detail synthesis procedure, methodologies and the corresponding characterizations are provided in Supporting Information (Fig. S1-S3).

2.3. Preparation of SII separator, SII-LE

0.07 g of SII was dissolved in 20 ml THF/MeOH (v/v = 1/1) mixed solvent. The SII solution was poured into a custom made glass dish with a diameter of 5 cm and the solvents were allowed to evaporate slowly at 40 °C. After vacuum drying and further thermal annealing at 120 °C for 24 h under vacuum to obtain the dry SII membrane. The electrolyte-filled SII separator (SII-LE) was prepared by immersing dry SII membrane in the electrolyte (1 M lithium fluorohexaphosphate ($LiPF_6$) in EC/DEC/EMC v/v/v = 4/3/3) at ambient temperature for 24 h before use.

2.4. Evaluation of thermal property and mechanical property

An Instruments Q600 was adopted for thermogravimetric analysis (TGA) with a heating rate of 10 °C min^{-1} under nitrogen atmosphere. The tensile tests were performed to evaluate the Young's modulus using a TA Instruments Q800. Before the experiment started, samples were first equilibrated at 40 °C for 10 min, and then a ramp force of 0.1 N min^{-1} was applied. Young's modulus was measured at 2% offset yield with the corresponding tensile strength in the tensile stress-strain curve.

2.5. Identification of microstructure

TEM images of microtomed thin slices were recorded using a Hitachi H-7100 equipped with a Gatan Dual Vision CCD Camera at an accelerating voltage of 75 kV. Ultra-microtoming was carried out using Leica Ultracut UCT6 at room temperature. The thin slices were exposed to RuO_4 vapours for 3 min when staining was required. Scanning electron microscopy (SEM) images of lithium metal surface were retrieved from Hitachi S-4800 Field Emission Scanning Electron Microscope with Energy Dispersive X-ray Spectrometer QUANTAX Annular XFlash® QUAD FQ5060. SAXS measurements were performed at BL23A beamline at NSRRC (National Synchrotron Radiation

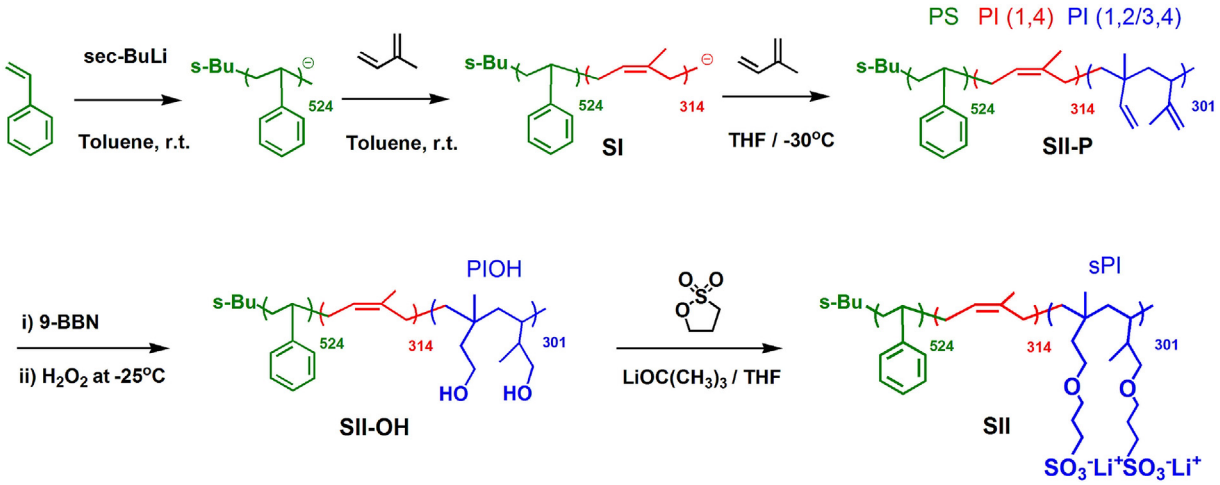

Fig. 1. Synthesis route of SII.

Research Center) of Taiwan in Hsinchu.

2.6. Ion transport property and galvanostatic cycling

Ionic conductivity (σ) was determined from the Nyquist plot of AC impedance experiment on a stainless steel symmetric cell (SSC) in the format of CR2032 coin cell. The SSC with cell structure of stainless steel/Separator-LE/stainless steel was assembled in a glove box infilling with Argon. The AC impedance experiment was performed with a voltage amplitude of 10 mV over the frequency range from 7Mz to 100 Hz. Lithium transference number (T_{Li}^{+}) was obtained from the Bruce and Vincent method on a Li/Separator-LE/Li cell according to the literature [34]. The cell was assembled in the glove box following the same procedure for SSC. All the electrochemical measurements were carried out using a Biologic SP-200 Potentiostat/Galvanostat/FRA. The galvanostatic cycling experiment was performed on a Li/Separator-LE/Li cell using a Biologic VMP3 Potentiostat/Galvanostat/FRA with repeating cycles of 3 h charging and 3 h discharging at 1 mA cm^{-2} current density in each cycle.

3. Results and discussion

3.1. Synthesis of SII and preparation of SII separator

SII triblock copolymer was synthesized by anionic polymerization and the succeeding analogous chemistry following the routes illustrated in Fig. 1. Anionic polymerization with sequential monomer addition and solvent/temperature change were employed to produce the precursor SII-P with narrow polydispersity index (PDI) [35]. The number average molecular weights (M_n) of PS, PI(1,4) and PI(1,2/3,4) in SII-P are 54000, 21000 and 20500 g mol^{-1} respectively. SII-P was then subjected to hydroboration/oxidation [36,37] and sulfo-propylation processes [38–40] to produce SII. A non-porous SII membrane was obtained by solvent casting from a solution of SII in THF/methanol. The photo of the bending SII membrane depicted in Fig. 3(a) clearly demonstrates the flexibility and the robustness of SII as a free standing membrane. To investigate the properties of the SII membrane absorbing liquid electrolyte, SII was immersed in LE for 24 h to afford a liquid electrolyte saturated separator, termed as SII-LE. The LE uptake was determined to be 30 wt%, much smaller than that (110 wt%) of the mesoporous Celgard 2320 saturated with LE (Celgard-LE) prepared from the same procedure because of the absence of pores. The photo of SII-LE revealed in Fig. 3(d) suggests SII could retain the integrity and the dimensional stability after saturation with LE.

3.2. Mechanical and thermal properties of SII separator

The mechanical strength of SII was evaluated by tensile stress-strain studies at 40 °C, in which a Young's modulus of 295 MPa was observed. This value is comparable with 345 MPa of Celgard 2320, indicating SII is sturdy enough to withstand the assembly process of cells. The thermal degradation temperature (T_d) of SII is 271 °C according to the temperature corresponding to a 5 wt% weight loss in TGA studies (Fig. S5), which suggests that SII is thermally stable at ambient operation temperature of LMB.

3.3. Microstructure of SII separator

SEM studies with EDS analysis were performed to identify the non-porous structure and the uniformity of the SII membrane, whose results are shown in Fig. 2 with Celgard separator as references. For Celgard, pores in micrometers could be clear observed from both surface (Fig. 2(a)) and cross-sectional images (Fig. 2(d)). By contrary, densely packed membrane was observed without detectable pores/holes in the SII cross-sectional image (Fig. 2(b) (e)). A very small amount of holes in nanometer scale were found in the SII surface image, probably due to the formation of bubbles during membrane casting. The SEM images should clearly demonstrate the non-porous structure of SII membrane. Of course, there should exist free volume in the nano- or sub-nanometer range within the membrane to allow the non-porous membrane to absorb liquid electrolytes, but it is typically not considered as porosity. Interestingly, we also observed the microphase-separated nanostructure showing twisted cylinders in the SII surface image with higher amplification, which is in consistency with the observation from TEM and SAXS studies as discussed below. The EDS analysis showed that SO_3Li groups (the origin of S signal) were homogeneously distributed within the SII membrane. All these results could further confirm the homogeneity of the microstructure throughout the membrane.

The morphological information in nanometer scale was extracted from the TEM image (Fig. 3(b)) and the SAXS pattern (Fig. 3(c)) of SII. In Fig. 3(b) where the dark regions representing PS rich domains and the bright regions indicating sPI segments, both dark and bright regions appear as short twisted cylinders and interpenetrate with each other. In Fig. 3(c) plotting $I \times q^2$ vs. q, a weak scattering peak at very low q (= 0.016 $Å^{-1}$) is observed, suggesting the existence of microphase separation while lack of long range order. Accordingly, we adopt a mass fractal model to fit the SAXS profile (Fig. S4) and find that a dense fractal network, suggesting a network of branched channels, is formed by the aggregation of the primary particles as basic unit (i.e., the smallest PS nano-domains). We hereby conclude that SII should exhibit a bicontinuous microphase separated structure with interpenetrated PS

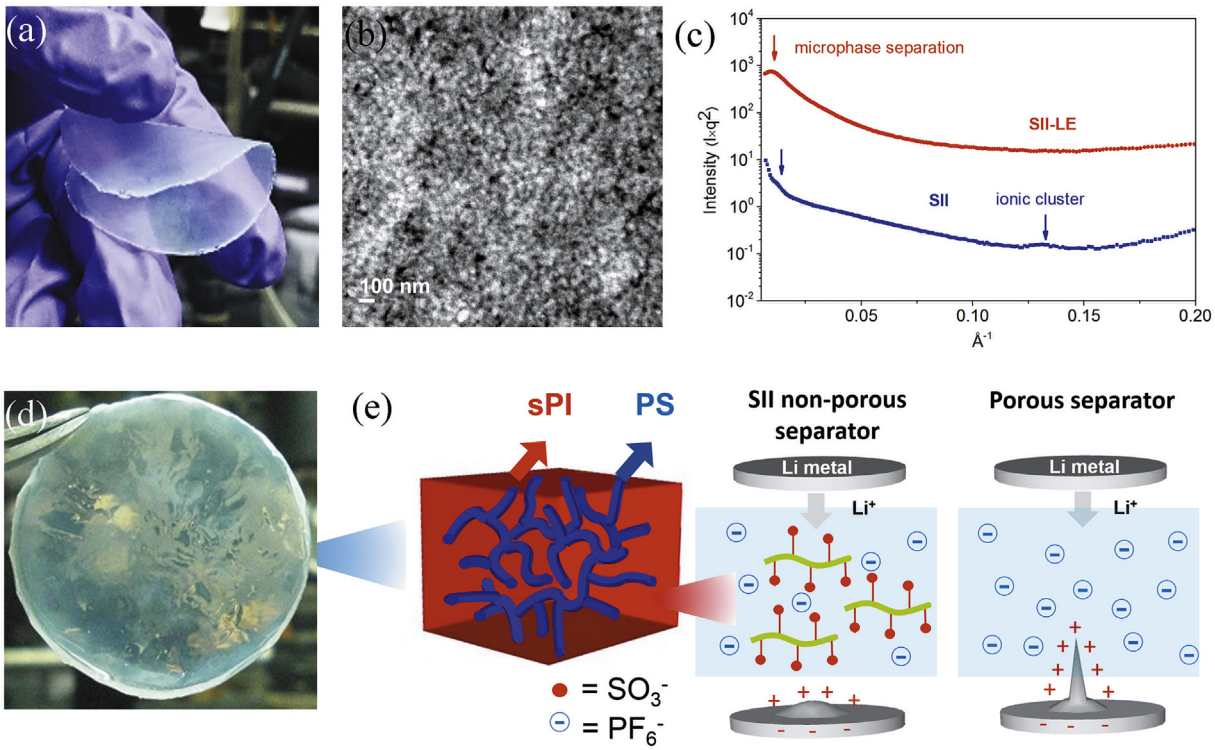

Fig. 2. (a) Photograph of bended SII separator; (b) TEM image of RuO4 stained thin slice of SII; (c) SAXS profile of SII separator and SII-LE; (d) Photograph of SII-LE; and (e) schematic illustration of the microstructure of SII separator and the proposed electrochemical deposition behavior of lithium ions in the lithium symmetrical cell comprised of SII-LE and Celgard –LE.

and sPI networks, as schematically illustrated in Fig. 3(e). According to the literature [41], ion conduction within a bicontinuous network might be the most effective since ions could transport through three-dimensional pathways without experiencing grain boundaries. As compared to SII, the SAXS pattern of SII-LE (Fig. 3(c)) reveals a broader peak at a lower q range with slightly decreased intensity, implying SII-LE should retain a microphase separated morphology similar to SII while possessing a slightly increased domain size. Hence, we reasonably suggest that the absorbed LE should preferentially occupy the free volume in the sPI domains to allow SII-LE preserve the bicontinuous network microstructure [36–47].

Table 1
Electrochemical properties.

Separator	σ (S cm^{-1})[a]	T_{Li}^+
SII-LE	1.45×10^{-4}	0.92
Celgard with 30% LE	Insulator	N/A[b]
Celgard with 110% LE	3.35×10^{-4}	0.28

[a] Conductivity and T_{Li}^+ were measured at room temperature.
[b] Not available.

3.4. Transport and electrochemical properties of SII-LE

The ion transport properties of SII-LE, including ionic conductivity (σ) and lithium transference number (T_{Li}^+) are summarized in Table 1.

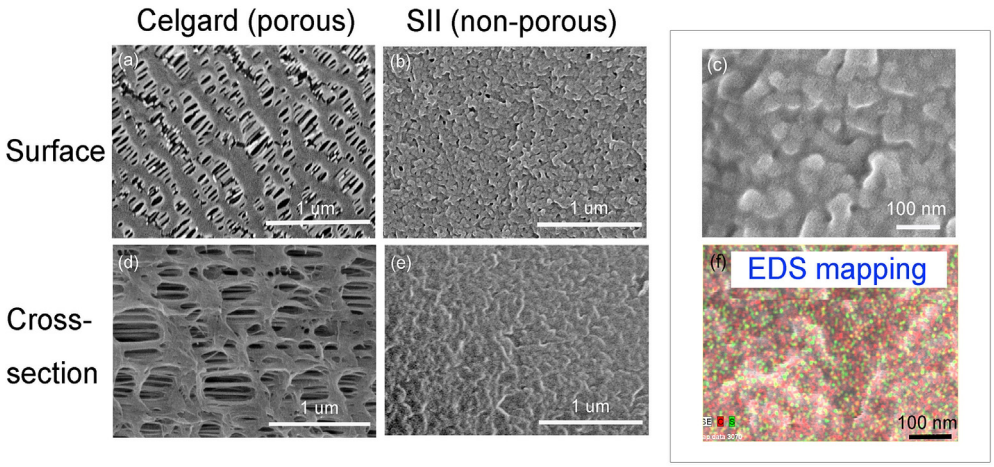

Fig. 3. SEM images of Celgard and SII separators: (a) (b) at surface, and (d) (e) at cross-section; (c) at surface with higher magnification (x 200000) and (f) the corresponding EDS mapping of sulfur (S) in (c).

The thickness of the SII membrane was controlled at 45 μm. Although it is not identical to 20 μm of Celgard, we think these thicknesses should be within comparable range especially when discussing the lithium ion transport properties as well as the electrodeposition and stripping behaviors of the lithium metal electrode. σ of SII-LE reaches 1.45×10^{-4} S cm^{-1} at room temperature as retrieved from the EIS measurement (Fig. S6). By contrast, Celgard with comparable LE uptake (~30 wt%) behaves virtually as an insulator for ion conduction because of insufficient LE to fulfill the pores of Celgard. On the other hand, the LE saturated Celgard (Celgard-LE) required a much higher LE uptake of 110 wt% to give a slightly higher conductivity of 3.35×10^{-4} S cm^{-1}. T_{Li}^{+} of SII-LE determined from Bruce and Vincent method is 0.92, much higher than 0.28 for Celgard-LE (Fig. S7). The value for Celgard-LE is typical for liquid electrolytes, generally around 0.3–0.4. The exceptionally high T_{Li}^{+} in SII-LE originated from the immobilized sulfonates anchoring onto the sPI backbone and the low LE content. According to Chazalviel's model, the time required for the nucleation of lithium dendrite (τ_s) is proportional to the inverse square of anion transference number (T_a^{-}) as suggested by Sand's law [26]. Since $T_a^{-} = 1 - T_{Li}^{+}$, the elevation of T_{Li}^{+} indicates the decrement of T_a^{-} and thus the elongation of τ_s. The high T_{Li}^{+} in SII-LE should substantially delay the nucleation of dendrite and therefore suppress lithium dendrite growth to improve the stability of lithium anode [28]. Taking gel electrolytes for comparison because both SII-LE and gel electrolytes are comprised of polymer and liquid electrolytes and lack of pores, SII-LE are much more sturdy than gel electrolytes to afford suitable mechanical properties for processing, dendrite blocking as well as long term integrity and dimensional stability [23]. Besides, T_{Li}^{+} of gel electrolytes are generally much smaller (~0.3–0.4) than that of SII-LE. Therefore, SII-LE should possess a higher potential than gel electrolytes to suppress lithium dendrite growth. The cyclic voltammetry on a Li/SII-LE/Al cell from 2.5 V to 5.2 V was performed to evaluate the electrochemical stability of SII-LE within the operation range of a lithium metal battery (Fig. S8). The result indicated no obvious redox peak within this voltage range, suggesting that SII-LE should be compatible with mostly adopted cathode and lithium metal anode.

3.5. Electrodeposition and stripping at lithium metal surface

The lithium electrodeposition and stripping behaviors at the interface between lithium metal and the separator were investigated by galvanostatic cycling experiments on a Li/SII-LE/Li cell at 1 mA cm^{-2} and room temperature. The cycling experiments were performed on both cells for 245 h in order to visualize the electrodeposited lithium surfaces for direct comparison. The corresponding profiles of overpotential (E) vs. time are depicted in Fig. 4(a). For SII-LE, the potential profile mostly appeared as a square wave with completely flat plateaus for deposition and stripping, suggesting constantly smooth lithium metal surface as a result of homogeneous stripping/deposition of lithium. By contrast, the potential profile of the Celgard-LE cell constantly showed curved plateaus with spiked edges for the stripping/deposition process, indicating the unevenness of the lithium metal surface. It is also noted that the potential retained a steady value for SII-LE, indicating the SEI film was not thickened before we stopped the galvanostatic cycling experiment. On the other hand, Celgard-LE showed a gradual increase in the potential with increasing cycle number, suggesting the increment in the interfacial resistance due to the thickening of SEI film as a result of progressively decomposition of the carbonate solvent of LE [44,45]. To examine the lithium cycle lifetime of SII-LE to evaluate the long term stability, galvanostatic cycling was performed on another Li/SII-LE/Li cell at 1 mA cm^{-2} and the associated potential profile is illustrated in Fig. 4(b). The overpotential profiles remained flat plateau even when the cycling time approached 500 h.

SEM images and photos of the lithium metal surfaces of Li/Separator-LE/Li cells after 245 h galvanostatic cycling are illustrated in Fig. 5. A smooth and flat surface without any distinctive irregular particles was observed for Li/SII-LE/Li as shown in Fig. 5(a). Oppositely, a rough and non-uniformed topography with distorted faceted particles in irregular shapes was found for Li/Celgard-LE/Li (Fig. 5(b)). Additionally, the lithium metal surface in contact with SII-LE is relatively bright and smooth (Fig. 5(c)) whereas that with Celgard-LE appeared dark and rough, as illustrated in Fig. 5(d).

XPS measurements were carried out to study the chemical composition of the lithium metal surfaces of Li/SII-LE/Li and of Li/Celgard-LE/Li cells after short circuit upon galvanostatic cycling. In the C 1s spectra shown in Fig. 6, three peaks locating at 284.2, 285.8, and 289.3 eV are observed, and which are associated with C-H species, lithium-alkyl carbonate ($ROCO_2Li$), and Li_2CO_3 respectively as typical products from the reduction of cyclic carbonates [46,47]. It can be seen that the intensities of $ROCO_2Li$ and Li_2CO_3 peaks for the SII-LE cell are significantly lower than those for the Celgard-LE cell, indicating the decomposition of the carbonate solvents in SII-LE is effectively suppressed in the SII-LE cell. In addition, no signals were detected in S 2p spectra for the SII-LE cell, suggesting the lithium sulfonates in SII should be stable upon galvanostatic cycling. Based on the galvanostatic cycling and the surface analysis results, we can conclude that SII-LE facilitates flat, uniform and stable interfaces between the lithium electrode and the separator to enable homogeneous lithium stripping/platting to impede dendrite formation.

4. Conclusion

In summary, a novel triblock copolymer SII bearing pendant lithium sulfonates with designated molecular architecture is successfully synthesized. A mechanical robust non-porous SII separator is prepared by solvent casting from a SII solution, and which possesses a bicontinuous microphase separated nanostructure with interconnected sPI domain for effective lithium ion conduction. With only 30 wt% LE uptake, the LE saturated separator SII-LE exhibits an ion conductivity of 1.45×10^{-4} S cm^{-1} and a high T_{Li+} of 0.92 at room temperature, along with good electrochemical stability. Over 500 h lithium cycle lifetime is achieved in the galvanostatic cycling at 1 mA cm^{-2} and room temperature of the Li/SII-LE/Li cell. The corresponding overpotential profiles as well as the SEM studies and XPS results suggest SII-LE could facilitate homogeneous electro-deposition and stripping at the interfaces between SII-LE and the lithium metal, resulting in flat lithium surfaces to impede dendrite formation.

Acknowledgment

This work is financially supported by Material and Chemical Research Laboratories, Industrial Technology Research Institute of Taiwan; by the “Advanced Research Center for Green Materials Science and Technology” from The Featured Area Research Center Program within the framework of the Higher Education Sprout Project by the Ministry of Education (107L9006) and the Ministry of Science and Technology in Taiwan (MOST107-3017-F-002-001) The authors gratefully acknowledge Prof. Chia Chin Chang in Department of Green Energy in National University of Tainan and Prof. Craig B. Arnold in Princeton Institute for the Science and Technology of Materials for their helpful discussions on the experimental results. We also thank Dr. Chia-Chin Chen in Max Planck Institute for Solid State Research for his pragmatic suggestions on experimental assistance. The XPS characterization was conducted in Research Center for Applied Science, Academia Sinica sponsored by Prof. Jing-Jong Shyue. The authors would also thank Mrs. Ching-Yen Lin and Mrs. Ya-Yu Yang in Instrumentation Center at National Taiwan University for the photography of SEM images.

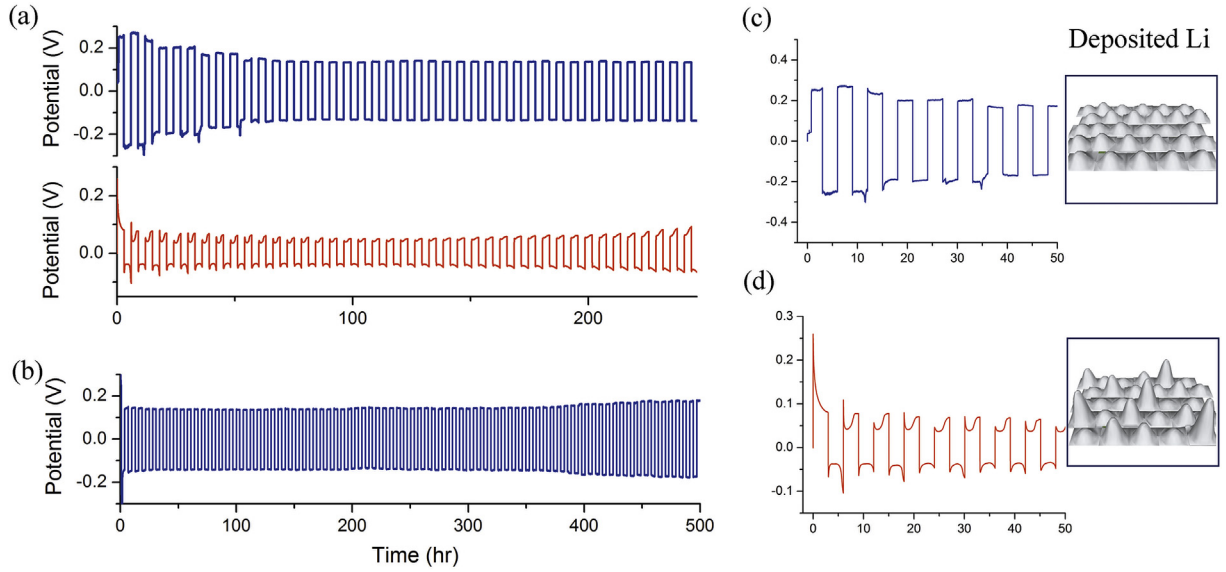

Fig. 4. Overpotential profiles of galvanostatic cycling at 1 mA cm^{-2} of (a) SII-LE and Celgard-LE up to 245 h, (b) SII-LE up to 500 h; and (c) (d) a closer look of initial cycles and the corresponding schematic illustration of lithium ion deposition.

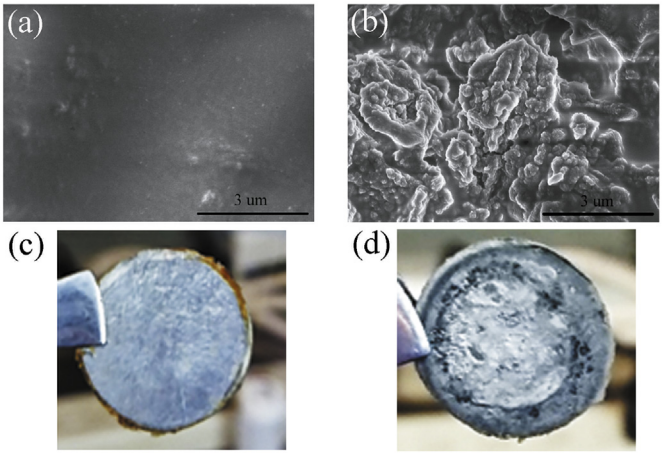

Fig. 5. SEM images and photographs of lithium metal surface of Li/Separator-LE/Li cells comprised of (a) (c) SII-LE; and (b) (d) Celgard-LE after 245 h galvanostatic cycling.

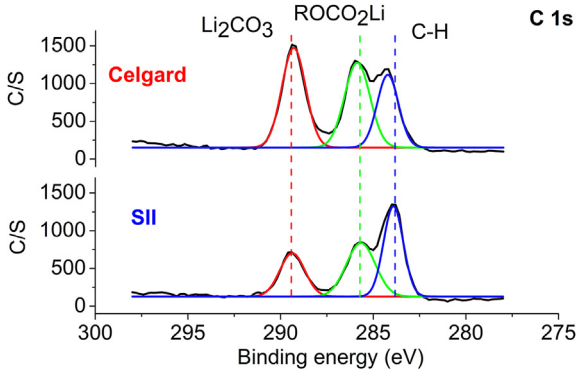

Fig. 6. XPS spectra in the energy range of C 1s signal of Li/Separator-LE/Li cell upon galvanostatic cycling for 245 h.

Nomenclature

Membrane preparation and composition

SII-P	Poly(styrene-*block*-isoprene(1,4)-*block*-isoprene(3,4)) tri-block copolymer
SII-OH	The precursor of SII with pendant hydroxyl groups
SII-OAc	End-capped SII-OH
SII	Single ion conducting triblock copolymer membrane
LE	Liquid electrolyte, 1 M lithium fluorohexaphophate ($LiPF_6$) in EC/DEC/EMC v/v/v = 4/3/3
SII-LE	SII membrane saturated with liquid electrolyte
Celgard	Celgard membrane
Celgard-LE	Celgard membrane saturated with liquid electrolyte

Appendix A. Supplementary data

Supplementary data to this article can be found online at https://doi.org/10.1016/j.jpowsour.2019.02.048.

References

[1] J.M. Tarascon, M. Armand, Nature 414 (2001) 359–367.
[2] R. Marom, S.F. Amalraj, N. Leifer, D. Jacob, D. Aurbach, J. Mater. Chem. 21 (2011) 9938–9954.
[3] M.M. Thackeray, C. Wolverton, E.D. Isaacs, Energy Environ. Sci. 5 (2012) 7854–7863.
[4] W. Xu, J.L. Wang, F. Ding, X.L. Chen, E. Nasybutin, Y.H. Zhang, J.G. Zhang, Energy Environ. Sci. 7 (2014) 513–537.
[5] Z.Y. Tu, P. Nath, Y.Y. Lu, M.D. Tikekar, L.A. Archer, Accounts Chem. Res. 48 (2015) 2947–2956.
[6] H. Ota, X.M. Wang, E. Yasukawa, J. Electrochem. Soc. 151 (2004) A427–A436.
[7] M.H. Ryou, D.J. Lee, J.N. Lee, Y.M. Lee, J.K. Park, J.W. Choi, Adv. Energy Mater. 2 (2012) 645–650.
[8] M.H. Ryou, Y.M. Lee, Y.J. Lee, M. Winter, P. Bieker, Adv. Funct. Mater. 25 (2015) 834–841.
[9] C.P. Yang, Y.X. Yin, S.F. Zhang, N.W. Li, Y.G. Guo, Nat. Commun. 6 (2015).
[10] X.B. Cheng, T.Z. Hou, R. Zhang, H.J. Peng, C.Z. Zhao, J.Q. Huang, Q. Zhang, Adv. Mater. 28 (2016) 2888–2895.
[11] Y. Liu, D. Lin, Z. Liang, J. Zhao, K. Yan, Y. Cui, Nat. Commun. 7 (2016) 10992.
[12] J. Park, J. Jeong, Y. Lee, M. Oh, M.H. Ryou, Y.M. Lee, Adv. Mater. Interfaces 3 (2016).
[13] J. Qian, W.A. Henderson, W. Xu, P. Bhattacharya, M. Engelhard, O. Borodin, J.-G. Zhang, Nat. Commun. 6 (2015) 6362.
[14] C. Zu, N. Azimi, Z. Zhang, A. Manthiram, J. Mater. Chem. 3 (2015) 14864–14870.
[15] E. Kazyak, K.N. Wood, N.P. Dasgupta, Chem. Mater. 27 (2015) 6457–6462.
[16] H. Lee, D.J. Lee, Y.J. Kim, J.K. Park, H.T. Kim, J. Power Sources 284 (2015)

103–108.
[17] D. Aurbach, B. Markovsky, G. Salitra, E. Markevich, Y. Talyossef, M. Koltypin, L. Nazar, B. Ellis, D. Kovacheva, J. Power Sources 165 (2007) 491–499.
[18] F. Marchioni, K. Star, E. Menke, T. Buffeteau, L. Servant, B. Dunn, F. Wudl, Langmuir 23 (2007) 11597–11602.
[19] G.A. Umeda, E. Menke, M. Richard, K.L. Stamm, F. Wudl, B. Dunn, J. Mater. Chem. 21 (2011) 1593–1599.
[20] F. Ding, W. Xu, G.L. Graff, J. Zhang, M.L. Sushko, X.L. Chen, Y.Y. Shao, M.H. Engelhard, Z.M. Nie, J. Xiao, X.J. Liu, P.V. Sushko, J. Liu, J.G. Zhang, J. Am. Chem. Soc. 135 (2013) 4450–4456.
[21] Y.Y. Liu, D.C. Lin, Z. Liang, J. Zhao, K. Yan, Y. Cui, Nat. Commun. 7 (2016).
[22] J.Y. Song, Y.Y. Wang, C.C. Wan, J. Power Sources 77 (1999) 183–197.
[23] A. Manuel, Stephan, Eur. Polym. J. 42 (2006) 21–42.
[24] K. Liu, P. Bai, M.Z. Bazant, C.-A. Wang, J. Li, J. Mater. Chem. 5 (2017) 4300–4307.
[25] Y.Y. Lu, M. Tikekar, R. Mohanty, K. Hendrickson, L. Ma, L.A. Archer, Adv. Energy Mater. 5 (2015) 1402073.
[26] J.N. Chazalviel, Phys. Rev. 42 (1990) 7355–7367.
[27] C. Monroe, J. Newman, J. Electrochem. Soc. 150 (2003) A1377–A1384.
[28] M.D. Tikekar, S. Choudhury, Z. Tu, L.A. Archer, Nature Energy 1 (2016) 16114.
[29] K. Liu, A. Pei, H.R. Lee, B. Kong, N. Liu, D. Lin, Y. Liu, C. Liu, P.-c. Hsu, Z. Bao, Y. Cui, J. Am. Chem. Soc. 139 (2017) 4815–4820.
[30] M.D. Tikekar, L.A. Archer, D.L. Koch, J. Electrochem. Soc. 161 (2014) A847–A855.
[31] M.D. Tikekar, L.A. Archer, D.L. Koch, Sci. Adv. 2 (2016) 7.
[32] J. Song, H. Lee, M.-J. Choo, J.-K. Park, H.-T. Kim, Sci. Rep. 5 (2015) 14458.
[33] J. Luo, R.C. Lee, J.T. Jin, Y.T. Weng, C.C. Fang, N.L. Wu, Chem. Commun. 53 (2017) 963–966.
[34] J. Evans, C.A. Vincent, P.G. Bruce, Polymer 28 (1987) 2324–2328.
[35] S. Bywater, Y. Firat, P.E. Black, J. Polym. Sci., Polym. Chem. Ed. 22 (1984) 669–672.
[36] T.C. Chung, M. Raate, E. Berluche, D.N. Schulz, Macromolecules 21 (1988) 1903–1907.
[37] G.P. Mao, J.G. Wang, S.R. Clingman, C.K. Ober, J.T. Chen, E.L. Thomas, Macromolecules 30 (1997) 2556–2567.
[38] N.S. Choi, Y.M. Lee, B.H. Lee, J.A. Lee, J.K. Park, Solid State Ionics 167 (2004) 293–299.
[39] J. Sun, P. Bayley, D.R. MacFarlane, M. Forsyth, Electrochim. Acta 52 (2007) 7083–7090.
[40] M.P. Kulkarni, T.J. Peckham, O.D. Thomas, S. Holdcroft, J. Polym. Sci., Polym. Chem. Ed. 51 (2013) 3654–3666.
[41] M. Chintapalli, X.C. Chen, J.L. Thelen, A.A. Teran, X. Wang, B.A. Garetz, N.P. Balsara, Macromolecules 47 (2014) 5424–5431.
[42] S.H. Chung, K. Such, W. Wieczorek, J.R. Stevens, J. Polym. Sci. B Polym. Phys. 32 (1994) 2733–2741.
[43] C.L. Campion, W. Li, B.L. Lucht, J. Electrochem. Soc. 152 (2005) A2327–A2334.
[44] M.S. Park, S.B. Ma, D.J. Lee, D. Im, S.-G. Doo, O. Yamamoto, Sci. Rep. 4 (2014) 3815.
[45] G. Bieker, M. Winter, P. Bieker, Phys. Chem. Chem. Phys. 17 (2015) 8670–8679.
[46] D. Aurbach, B. Markovsky, A. Shechter, Y. Ein-Eli, H. Cohen, J. Electrochem. Soc. 143 (1996) 3809–3820.
[47] E.M. Erickson, E. Markevich, G. Salitra, D. Sharon, D. Hirshberg, E. de la Llave, I. Shterenberg, A. Rosenman, A. Frimer, D. Aurbach, J. Electrochem. Soc. 162 (2015) A2424–A2438.